Exploring the chiral regime of QCD in the interacting instanton liquid model

M. Cristoforetti, P. Faccioli, and M. C. Traini

Dipartimento di Fisica and I.N.F.N., Università degli Studi di Trento, Via Sommarive 15, Povo (Trento) 38050 Italy.
and European Centre for Theoretical Studies in Nuclear Physics and Related Areas,
Strada delle Tabarelle 286, Villazzano (Trento), I-38050 Italy.

J. W. Negele

Center for Theoretical Physics Massachusetts Institute of Technology,
NE25-4079, 77 Massachusetts Ave, Cambridge, Massachusetts 02139-4307, USA.

The interacting instanton liquid model (IILM) is used to explore the role of instanton-induced dynamics in hadron structure. To support the validity of this model in the chiral regime, the quark mass dependencies of several properties are shown to agree with chiral perturbation theory, including the density of eigenmodes of the Dirac operator and the mass of the pion. A quark mass $m^* = 80$ MeV emerging naturally from the model is shown to specify the mass scale above which the fermion determinant is suppressed, the zero modes become subdominant, and the density of quasizero modes become independent of the quark mass.

I. INTRODUCTION

The goal of this work is to gain insight into the mechanism by which the structure of hadrons arises from QCD. Although lattice field theory provides a powerful tool for solving nonperturbative QCD and is now beginning to successfully calculate experimental observables with dynamical quarks in the chiral regime, the physical mechanism by which hadron structure arises and the dominant degrees of freedom are not directly evident. Hence, in this work, we explore the complementary insight that can be obtained from a model that focuses on what we believe to be the dominant degrees of freedom relevant to hadron structure. In nonperturbative QCD, the way in which gluons interact with quarks depends dramatically on the quark mass. In the limit of large mass, heavy quarks move adiabatically in a flux tube potential, whereas in the limit of light mass, a variety of evidence suggests that the instanton-induced 't Hooft quark interaction plays an important role and provides the mechanism for spontaneous chiral symmetry breaking. To understand the structure of hadrons containing light up and down quarks, we therefore seek to explore the role of instantons and their associated zero modes in hadron structure, and do so in the context of the interacting instanton liquid model (IILM).

In the IILM, the QCD path integral over all gluons is replaced by an effective theory in which instantons are the effective degrees of freedom, and the gauge fields of the theory are those generated by integrating over the positions, color orientations, and sizes of instantons. In the context of this model, we would like to understand the mass range in which instanton mediated chiral dynamics is manifested and the extent to which it is described by chiral perturbation theory. In particular, we would like to know the mass scale or scales at which the continuum fermion

determinant is suppressed, at which zero modes become subdominant, and at which the density of quasi zero modes becomes independent of quark mass.

In the present paper, we set-up the formalism to use the IILM [1] to address these questions. The instanton picture (for recent reviews see [2,3]) was originally introduced as a model for the QCD vacuum based on semiclassical arguments [4]. It was shown that instantons lead to spontaneous chiral symmetry breaking by introducing strong nonpertrubative correlations between fermionic zero-modes localized around the instanton positions. Specific features of the instanton picture have been observed in a number of lattice studies [5–9] and there is evidence that chiral symmetry breaking is correlated with smooth lumps of topological charge, whose profile is consistent with that of singular-gauge instantons [10,11]. In addition, instanton-induced correlations in hadrons have been studied in a number of phenomenological model calculations, where it was shown that the Instanton Liquid Model, (ILM), provides a good description of the mass and the electro-weak structure of pions, nucleons and hyperons [12–21].

Before trusting the IILM to provide useful insight into the role of instantons and their associated zero modes, it is important to verify several essential properties. One key issue is to verify the chiral behavior of the spectrum of the Dirac operator. By analyzing the dependence on the quark mass of the density of eigenvalues of the Dirac operator, $\rho(\lambda)$. we show that, in the chiral limit, the IILM results are consistent with the well-known chiral perturbation theory (χpt) result [22]:

$$\lim_{\lambda \to 0} \lim_{m_q \to 0} \rho(\lambda) = \text{Const} + O(\lambda^2) \qquad (N_f = 2). \quad (1)$$

In addition, we check that at small but-finite quark masses,

the IILM generates mass corrections to the Dirac spectrum that are consistent with those predicted by χpt. To do so, we show that from the structure of the IILM Dirac spectrum computed at different quark masses, one can predict the power-law infrared divergence in the quark mass of the scalar three-point correlator:

$$K^{abc} \equiv \int d^4x d^4y d^4z \langle 0|S^a(x)S^b(y)S^c(z)|0\rangle \propto \frac{1}{m_q}, \quad (2)$$

$$S^a(x) = \bar{q}(z)\tau^a q(x). \quad (3)$$

This result agrees with the prediction of χpt [22]:

$$K^{abc} = \frac{B^3(N_f^2 - 12)}{64\pi^2 m_\pi^2 N_f} d^{abc} + O(p^4) \propto \frac{1}{m_q}. \quad (4)$$

A second important test is verifying that the IILM effective theory can be used to calculate hadron masses and that these masses have the dependence on the quark mass expected from χpt. Since correlation functions in the nucleon and pion channels receive contributions from a single instanton whereas in the ρ and Δ channels the leading contribution occurs for two instantons, the nucleon and pion masses depend on the instanton density to first order while the ρ and Δ are only affected in second order. Hence, we focus here on the nucleon and pion masses. Since we have replaced the functional integral over all gluon fields by a sum over instanton fields, a key task is to verify that the effective theory is an adequate approximation to the full functional by showing that the correlation function decays at large Euclidean time like a pure exponential, as it must in a field theory with a transfer matrix, and that spontaneous chiral symmetry breaking occurs as it would in the full field theory. In the case of the pion, we demonstrate very clear asymptotic decay as a single exponential and use the slope to obtain an accurate measurement of the pion mass at each quark mass. These data not only have a quark mass dependence consistent with the form expected from chiral perturbation theory, but we show that they yield low-energy constants consistent with those known from QCD. The nucleon is slightly more problematic, in the sense that with the Monte Carlo statistics accessible to us, the combined systematic and statistical errors are somewhat larger than in the pion case. We show that these data are completely consistent with recent lattice QCD calculations.

Having carefully verified the consistency of the IILM results with lattice results and with the behavior expected from χpt, we conclude that the low-energy effective theory indeed gives a useful approximation to the QCD path integral and hence use this model to explore the role of instanton-induced dynamics. An essential quantity in the IILM is the overlap matrix T_{ij} specifying the probability that a quark hops from instanton i to instanton j, and we find that a value of the quark mass m^* defined to be equal to an average value of T_{ij} is a key parameter in characterizing the

quark mass dependence of low-energy QCD. In the IILM, $m^* = 80$ MeV, corresponding to $m_\pi = 600$ MeV, and characterizes the scale for three transitions. It is the mass scale above which the fermion determinant is suppressed, the zero modes become subdominant, and the density of quasizero modes becomes independent of quark mass. The significance of these transitions is discussed in the text.

The paper is organized as follows. In the next section, we review some of the basic aspects of the IILM. In Sec. III, we present our analysis of the Dirac spectrum and compare our results with chiral perturbation theory predictions. In Sec. IV, we present the details of our calculations of hadron masses and compare our results with lattice data. In Sec. V, we perform chiral extrapolations of the pion masses and compare the effective parameters of the low-energy chiral perturbation theory of the IILM with those of QCD. In Sec. VI, we analyze how in the IILM the chiral dynamics is incorporated in the structure of the quark propagator and in the fermionic determinant, and we define and compute the mass scale $m^\star$ that sets the boundary of the chiral regime. All results are summarized in Sec. VII.

II. THE INTERACTING INSTANTON LIQUID MODEL

In the IILM, the QCD path-integral over the gauge field configurations is replaced by a sum over the configurations of a grand-canonical statistical ensemble of instantons and anti-instantons:

$$\begin{aligned} Z_{\text{QCD}} &\simeq Z_{\text{ILM}} \\ &= \sum_{N_+,N_-} \frac{1}{N_+!N_-!} \\ &\times \int \prod_i^{N_++N_-} d\Omega_i d(\rho_i) e^{-S_{\text{int}}} \prod_i^{N_f} \det(i\slashed{D} + im_f). \end{aligned}$$
(5)

Here, $d\Omega_i = dU_i d^4z_i d\rho_i$ is the measure in the space of collective coordinates, color orientation, position and size, associated with the single instantons. Quantum fluctuations are included in Gaussian approximation, through the semi-classical instanton amplitude $d(\rho_i)$. In what follows we will work in the thermodynamical limit and adopt the canonical formulation with $N_+ = N_- = N/2$.

Since instanton-instanton interactions are important to remove large-sized instantons from the vacuum [4], the partition function (5) describes an interacting liquid, rather than a dilute gas of pseudoparticles. The corresponding interaction action is defined as

$$S_{\text{int}} \equiv S_{\text{tot}} - (N_+ + N_-)S_0, \quad (6)$$

where S_{tot} is the total classical action corresponding to a

given ensemble configuration and $S_0 = \frac{8\pi}{g^2}$ is the individual single-instanton action in the dilute-gas limit.

In the IILM, the interaction action is approximated by a pure two-body instanton-anti-instanton term, which only depends on the relative coordinates of two pseudoparticles:

$$S_{\text{int}} = \frac{1}{2} \sum_{I \neq J}^{N/2} S_{\text{int}}(I, J) \tag{7}$$

Such a two-body action is calculated classically, by first determining the total action S_{tot} from the gauge potential $A_\mu(I, A)$ corresponding to the instanton-anti-instanton pair and then subtracting the free contribution $2S_0$. Since no exact instanton-anti-instanton pair solution $A_\mu(I, A)$ to the classical Yang-Mills equations of motion is known, we rely on the streamline construction, in which the classical action is minimized in all the directions except along the collective coordinate describing the separation between the two instantons [23]. The analytic instanton–anti-instanton gauge potential in the streamline *Ansatz* is given by

$$A_\mu^a = 2\eta_{\mu\nu}^a \frac{x_\nu}{x^2 + \rho^2\lambda} + 2R^{ab}\eta_{\mu\nu}^b \frac{\rho^2}{\lambda} \frac{1}{x^2(x^2 + \rho^2/\lambda)} \tag{8}$$

where λ is the streamline conformal parameter defined by

$$\lambda = \frac{R^2 + \rho_I^2 + \rho_A^2}{2\rho_I\rho_A} + \left(\frac{(R^2 + \rho_I^2 + \rho_A^2)^2}{4\rho_I^2\rho_A^2} - 1\right)^{1/2} \tag{9}$$

$$R = |z_I - z_A|$$

and

$$R^{ab} = \tfrac{1}{2}\text{Tr}[U^\dagger \tau^a U \tau^b] \tag{10}$$

represents the relative color orientation of the two instantons.

A major shortcoming of the streamline construction is that, in the most attractive color orientation channel, the interaction action smoothly approaches $S_{\text{int}} = -2S_0$ at short distances. This means that the instanton-anti-instanton pair tends to annihilate. The resulting gauge field configuration is characterized by a vanishing topological charge and a weak gauge field potential, and therefore it corresponds to a perturbative fluctuation. Since perturbative contributions cannot be treated consistently in the present approach, Shuryak and Schäfer [1] suggested removing them by introducing a purely phenomenological short-range repulsive core:

$$S_{\text{core}} = \frac{A}{\lambda^4} |u|^2, \tag{11}$$

where u is a color orientational factor. Such a term provides a cut-off to the momentum that can be exchanged through the instanton field, hence restricting the region of applicability of the approach to the nonperturbative sector characterized by momenta of the order $p < 1/\bar{\rho}$, where $\bar{\rho}$ is the average instanton size. In the language of effective field theory, this repulsive core plays the role of a counter-term, parametrizing the ultraviolet physics. However, it should be stressed that our hard-core is not derived from a systematic contruction and therefore introduces model dependence in the calculation. The coefficient A in (11) controls the strength of the repulsion and is the only phenomenological parameter of the model. In our calculations we adopted the value $A = 128$ suggested by Schäfer and Shuryak [1].

Once the interaction action is defined, it is possible to compute the main properties of the ensemble, the instanton density n, and instanton size distribution $d(\rho)$, by minimizing the ensemble's free energy numerically. One can then calculate arbitrary Euclidean Green functions by performing Monte Carlo averages over instanton configurations, using the Metropolis algorithm. As in analogous lattice QCD calculations, one must set the scale in physical units by matching one dimensionful quantity.

In order to compute correlation functions involving quark field operators, we follow the same prescription adopted in lattice simulations, i.e. we first explicitly integrate out the fermion fields and then compute Monte Carlo averages of the resulting Wick contractions. Such averages are performed using configurations which are obtained by an accept/reject Metropolis algorithm in which the contribution of the fermionic determinant is included in the Bolzmann weight, corresponding to unquenched simulations.

Unlike in lattice QCD simulations, where the fermionic determinant and the quark propagators are evaluated using a purely numerical algorithm, in the IILM these quantities have a semianalytic representation. This property allows us to identify the physical content of each term and establish a connection with the corresponding nonperturbative quark dynamics [2]. The fermionic determinant in a given instanton gauge field A_μ background is factorized into a contribution of near-zero modes and a contribution arising from nonzero modes:

$$\det_A(\slashed{D} + m_q) = \det_{Azm} \times \det'_{Anzm}. \tag{12}$$

The contribution of near-zero modes can be determined exactly, by expanding the Dirac operator on the basis of zero-modes of individual instantons:

$$\det_{Azm} = \det(T + m_q), \tag{13}$$

where $T_{IJ} = \int d^4z \, \psi_I^{0\dagger}(z) i D_\mu \gamma_\mu \psi_j^0(z)$ is the overlap matrix which represents the probability amplitude for quarks to "hop" from the instanton I to the instanton J. The nonzero mode part of the fermionic determinant is approximated with the product of the nonzero mode contributions of each individual instanton:

$$\det{}'_{Azm} = \prod_i^{N_+ + N_-} (1.34 m_q \rho_i) \tag{14}$$

Simlarly, the quark propagator consists of a zero-mode part and a nonzero mode part:

$$S(x, y)_A = S_{zm}(x, y)_A + S_{nzm}(x, y)_A. \tag{15}$$

The zero-mode part of the propagator $S_{zm}(x, y)_A$ dominates in the low-energy regime and encodes the information on the physics of chiral symmety breaking and axial anomaly saturation. It is constructed by representing the Dirac operator in the basis of zero-mode wave functions $\psi^0(x)$ of the individual instantons and reads:

$$S_{zm}(x, y)_A = \sum_{IJ} \psi_I^0(x) \psi_J^{0\dagger}(y) \left[\frac{1}{\hat{T} - im_q} \right]_{IJ}. \tag{16}$$

The non-zero-mode part is approximated as the sum of the non-zero-mode propagators in the field of the invidual instantons [2].

III. THE SPECTRUM OF THE DIRAC OPERATOR AND THE CHIRAL REGIME IN THE IILM

In the previous section, we have seen that the main approximation of the IILM consists in replacing the QCD path integral with a statistical sum over a classical ensemble of pseudoparticles. In this section, we address the question of whether such an approximation provides a realistic description of the nonperturbative quark-gluon dynamics associated with the spontaneous breaking of chiral symmetry in QCD. To this end we focus on the low-virtuality sector of the spectrum of the Dirac Operator $\slashed{D}$, which encodes information about the dynamics associated with the spontaneous breaking of chiral symmetry. Such a connection is made explicit in the Banks-Casher relation which relates the density of eigenvalues with small virtuality to the quark condensate:

$$\langle \bar{q}q \rangle = -\pi \rho(\lambda = 0), \tag{17}$$

We recall that this relation holds in a infinite-volume system and in the chiral limit. Our goal is to explore finite-mass corrections to the Banks-Casher relation in the instanton model and check if such corrections are consistent with predictions derived from χpt.

In order to set the framework of our analysis, it is useful to briefly review how the Banks-Casher relation (17) was obtained. The quark propagator $S(x, y)_A$ in the fixed background A_μ is expanded in terms of the eigenvalues λ and eigenvectors ψ_λ of the Dirac operator as

$$S(x, y)_A = \sum_n \frac{\psi_n(x) \psi_n^\dagger(y)}{m_q - i\lambda_n}. \tag{18}$$

Chiral symmetry implies that for every nonzero eigenvalue λ with eigenvector ψ_λ there is another eigenvalue $-\lambda$ with eigenvector $\gamma_5 \psi_\lambda$. Hence, setting $x = y$ and using the orthonormality of the basis of eigenfunctions of ψ_λ we obtain

$$\frac{1}{V} \int d^4x \, \text{Tr}[S(x, x)]_A = \frac{2m_q}{V} \sum_{\lambda_n > 0} \frac{1}{m_q^2 + \lambda_n^2} \tag{19}$$

Introducing the spectral density $\rho(\lambda) = \langle \sum_n \delta(\lambda - \lambda_n) \rangle$ we can rewrite (19) as

$$\langle \bar{q}q \rangle = -2m_q \int_0^\infty d\lambda \frac{\rho(\lambda)}{m_q^2 + \lambda^2} \tag{20}$$

At this point we take the limit $V \to \infty$ and $m \to 0$. We notice that the order in which the two limits are taken is crucial since we only have a finite quark condensate in the thermodynamic limit:

$$\langle \bar{q}q \rangle = \lim_{m_q \to 0} \lim_{V \to \infty} -2m_q \int_0^\infty d\lambda \frac{\rho(\lambda)}{m_q^2 + \lambda^2} = -\pi \rho(\lambda = 0). \tag{21}$$

Equation (17) can be interpreted as the lowest-order term in the Taylor expansion of $\rho(\lambda)$ near the origin, in the chiral limit. The next order in λ was derived by Smilga and Stern [22] using χpt:

$$\rho(\lambda) = -\frac{1}{\pi} B f_0^2 + \frac{B^2(N_f^2 - 4)}{32\pi^2 N_f f_0^2} |\lambda| + \mathcal{O}(\lambda), \tag{22}$$

where N_f is the number of flavors, B and f_0 are the constants that appear in the lowest-order χpt Lagrangian

$$\mathcal{L} = f_0^2 \left(\frac{1}{4} \text{Tr}[\partial_\mu U \partial^\mu U^\dagger] + 2B \, \text{Tr}[MU^\dagger + UM^\dagger] \right),$$

$U = \exp(i \frac{\phi(x)}{f_0})$, and M is the diagonal quark mass matrix.

We stress the fact that the result (22) is valid only in the limit in which the quark mass is much smaller than the typical eigenvalue saturating the spectral integral (20), $m_q \ll \lambda$. If the quark mass is of the order of the typical eigenvalue λ, then mass-dependent corrections to the spectral density profile are expected to appear. Hence, the question arises if there exists a range of masses for which the χpt predictions are accurate, yet mass corrections to (22) become important. In order to address this question, Smilga and Stern considered the 3-point scalar correlator:

$$K^{abc} = \int d^4x d^4y d^4z \langle 0|S^a(x)S^b(y)S^c(z)|0 \rangle, \tag{23}$$

where $S^a(x)$ is the scalar density operator, $S^a(x) = \bar{q}(x)\tau^a q(x)$. By proceeding in the same way as for the quark condensate they obtained an expression for K^{abc} in terms of the density of eigenvalues, $\rho(\lambda)$:

$$K^{abc} = -d^{abc} m_q \int_0^\infty \rho(\lambda) \frac{(m_q^2 - 3\lambda^2)}{(m_q^2 + \lambda^2)^3} d\lambda. \tag{24}$$

In the limit in which all mass corrections to (22) can be neglected, one can obtain a prediction for the 3-point scalar correlator by substituting the expansion of $\rho(\lambda)$ given in (22) in (24) and performing the integral. The constant term

in $\rho(\lambda)$ does not contribute, while the linear term gives rise to a power-law singularity in the pion mass:

$$K^{abc} = \frac{B^2(N_f^2 - 4)}{64\pi^2 N_f} \frac{1}{m_q} \propto 1/(m_\pi^2). \qquad (25)$$

On the other hand, evaluating the same correlator to lowest-order in χpt one finds:

$$K^{abc} = \frac{B^3(N_f^2 - 12)}{64\pi^2 m_\pi^2 N_f} d^{abc}. \qquad (26)$$

Note that, although in both cases one finds the same power-law dependence on the pion mass, the numerical coefficient turns out to be different

$$N_f^2 - 4 \neq (N_f^2 - 12)/2 \qquad (27)$$

The explanation of the mismatch is that the characteristic eigenvalues, λ, saturating the power divergent integral (24) are of order m_q, so we are out of the range of validity of (22). In order to reproduce the correct χpt prediction for the scalar 3-point correlator such mass corrections have to be included.

It is particularly interesting to consider the case $N_f = 2$, for which the linear term in (22) vanishes and the distribution of eigenvalues near the origin is flat. In this case, the power-law divergence in the pion mass predicted by χpt must arise entirely from mass corrections. This observation can be used to check the consistency of the IILM with χpt. We have performed simulations of the Dirac spectrum at different values of the quark mass, ranging from 0 to 400 MeV. The contribution of the near-zero-mode zone to the $N_f = 2$ spectral density of the positive eigenvalues is presented in Fig. 1.

Some comments on these results are in order. When the quark mass approaches zero, our results become consistent with the flat trend predicted by (22):

$$\lim_{m_q \to 0} \lim_{\lambda \to 0} \rho(\lambda) = \text{Const} + O(\lambda^2). \qquad (28)$$

The value of the constant depends on the normalization of the spectrum and can be fixed by imposing the condition (17). This case has been already considered in previous studies of Shuryak and Verbaarschot [24,25]. On the other hand, as the quark mass increases, the structure of the spectrum changes appreciably. The flatness near $\lambda = 0$ disappears and a peak near the origin develops. In Fig. 1 we see that for small λ, all curves at different masses are very well fitted with functions of the form $\rho(\lambda) - \rho(0) \propto m^\alpha \lambda^{1-\alpha}$. If this form is introduced in the spectral representation of the scalar three-point function (25), the integral can be carried out analytically leading to results proportional to the inverse quark mass.

To directly compare the χpt formula for K^{abc} with the results of IILM calculations, it is convenient to consider the combination $m_q \frac{K^{abc}}{\rho_{m=0}(0)}$. In fact, using the Gell-Mann Oaks
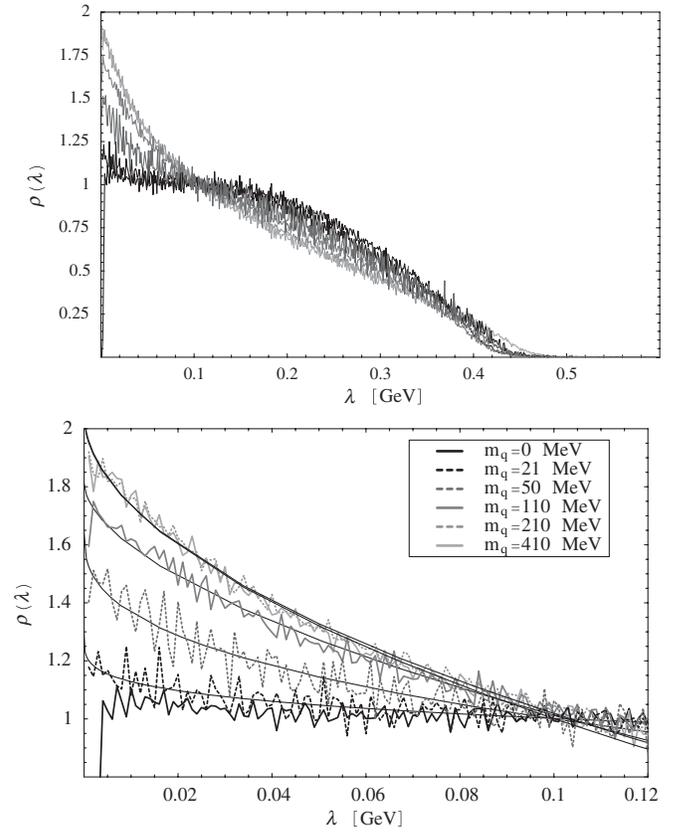
FIG. 1. Spectral density of the Dirac operator for $N_c = 3$ and $N_f = 2$. The lower panel shows an enlargement of the upper panel in the region $0 \leq \lambda \leq 0.3$ and the solid lines represent best fits using $\rho(\lambda) = c_1 + c_2 \times m_q^\alpha \lambda^{\alpha-1}$.

Renner and Banks-Casher relations, we find the simple χpt prediction

$$m_q \lim_{m_q \to 0} \frac{K^{abc}}{\rho_{m_q=0}(0)} = \frac{B(N_f^2 - 12)}{128\pi f_0^2 N_f} = \text{const}. \qquad (29)$$

On the other hand, from the spectral representation (24) we find

$$m_q \frac{K^{abc}}{\rho_{m_q=0}(0)} = -m_q^2 \int d\lambda \frac{\rho_{m_q}(\lambda)}{\rho_{m_q=0}(0)} \frac{(m_q^2 - 3\lambda^2)}{(m_q^2 + \lambda^2)^3} d^{abc},$$

which can be computed directly from our IILM points.

The results are plotted in Fig. 2, and we observe that the expected constant behavior with m is obtained for $m_q < 80$ MeV. Thus, in this case, the IILM reproduces the structure of the Dirac spectrum dictated by chiral symmetry.

IV. PION AND NUCLEON MASS IN THE IILM

In this section we present our IILM calculation of the nucleon and pion masses performed at different values of the quark masses and we compare with the available lattice results. Exploratory estimates of the nucleon and pion
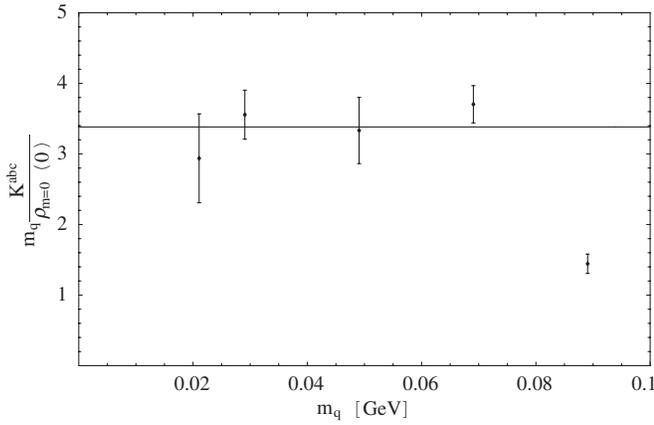
FIG. 2. $m_q \frac{K^{abc}}{\rho_{m=0}(0)}$ at different quark mass values in the IILM.

masses in the IILM were performed at a relatively large quark mass in [26]. However, such calculations were based on the analysis of short-range point-to-point Euclidean correlators and relied on a specific assumption for the spectral density (i.e. pole-plus-continuum parametrization). In the present work, we have chosen to avoid any *a priori* assumption on the spectral density. Instead, we have performed the effective-mass plot analysis, which is routinely used to extract the lowest-lying hadron masses from lattice QCD simulations.

To compute the mass of the pion, we have evaluated the correlation function:

$$G_\pi(\tau) = \int d^3\mathbf{x}\langle 0|T[j_5(\mathbf{x},\tau)\bar{j}_5(\mathbf{0},0)]|0\rangle, \qquad (30)$$

where $j_5(x)$ is the pseudoscalar density operator

$$j_5^a(x) = \bar{q}(x)\gamma_5\tau^a q(x). \qquad (31)$$

To compute the nucleon mass we have evaluated the correlation function

$$G_N(\tau) = \int d^3\mathbf{x}\langle 0|T[j_N(\mathbf{x},\tau)\bar{j}_N(\mathbf{0},0)P_+]|0\rangle, \qquad (32)$$

where $P_+ = \frac{1-\gamma_4}{2}$ is the positive-parity projector and

$$j_N^a(x) = \varepsilon^{abc}u^a(x)C\gamma_5 d^b(x)u^c(x). \qquad (33)$$

The integration over the final position $\mathbf{x}$ in (30) and (32) ensures projection onto zero-momentum states. The mass of these hadrons can then be extracted from the plateau in the large Euclidean time limit of the effective mass, i.e. using

$$M_{\pi/N} = \lim_{\tau\to\infty}M_{\pi/N}^{\text{eff}}(\tau) \qquad (34)$$

$$M_{\pi/N}^{\text{eff}}(\tau) = \frac{1}{\Delta\tau}\ln\frac{G_{\pi/N}(\tau)}{G_{\pi/N}(\tau+\Delta\tau)}. \qquad (35)$$

The point-to-point correlation functions in (30) and (32) were computed by performing Monte Carlo averages over

instanton ensemble configurations, as described in Sec. II. The momentum-projection integrals in (30) was carried out using an adaptive Monte Carlo routine (VEGAS) with two iterations of 6000 points. For the momentum-projection of the nucleon 2-point function (32) we combined the results of VEGAS with those obtained using a cubic grid with grid spacing 0.1 fm. Statistical errors over ensemble averages were obtained using the jackknife technique, with a bin size of 10 configurations. We have used five sets of 250 independent configurations corresponding to quark masses ranging from 20 to 90 MeV. In order to reduce finite volume artifacts, we performed our computations in two boxes of size $3.45^3 \times 5.9$ fm^4—for the two lightest quark masses—and $2.96^3 \times 5.9$ fm^4—for the other masses—. We have checked that with such a choice the condition $m_\pi L > 5$ was always satisfied.

All simulations where performed using the 1TFlop/s ECT* cluster, for a total computational time of 30000 cpu hours. In Fig. 3 we present pion and nucleon effective-mass plots for the different values of quark mass. We observe that the all pion effective-mass plots display a very clean plateau, from which it is possible to unambiguously read-off the pion mass from a correlated chi-square fit. On the other hand, the interpolation of the effective-mass plots of the nucleon is somewhat more problematic. In fact, not only statistical errors are larger, but also some of the plots are consistent with a slight slope, in the large Euclidean time regime. Hence, one necessarily needs to account for the systematic errors, which can be estimated from the smallest and largest mass compatible with the effective-mass plot, in the nearly flat region $\tau \gtrsim 1$ fm.

We recall that in the instanton model, the average instanton size $\bar{\rho}$ is the parameter determining the ultraviolet cut-off and playing the role of the lattice spacing a in lattice gauge theory. Hence, we have expressed all dimensional quantities in units of $\bar{\rho}$ and then determined it from a matching condition. For simplicity, we have chosen the condition that the IILM prediction for the nucleon mass should match the CP-PACS lattice result at the pion mass $m_\pi = 525$ MeV. The values of the nucleon masses for $m_\pi < 500$ MeV are therefore predictions of the model. The choice of the matching point was motivated by the fact that the pion mass $\simeq 500$ MeV represents an upper bound for the mass regime of QCD where the dynamics of chiral symmetry breaking is expected to play an important role.

In Fig. 4 we present the results of our calculations for the nucleon mass as a function of the pion mass squared for different choices of the cut-off $\bar{\rho}$. Comparing these IILM data at different $\bar{\rho}$ with the lattice data collaborations [27,28] clearly shows that agreement between IILM and lattice QCD predictions is obtained only for a unique value of the cut-off scale, corresponding to an average instanton size of 0.32 fm, in excellent agreement with the early phenomenological estimate $\bar{\rho} \simeq 1/3$ fm [4] and recent

lattice results [6,29–32]. The complete set of values of masses extracted from our IILM calculations is presented in Table I.

In Fig. 5 we can see that the IILM extracted nucleon masses are compatible with the available Lattice date for the pion mass range considered.
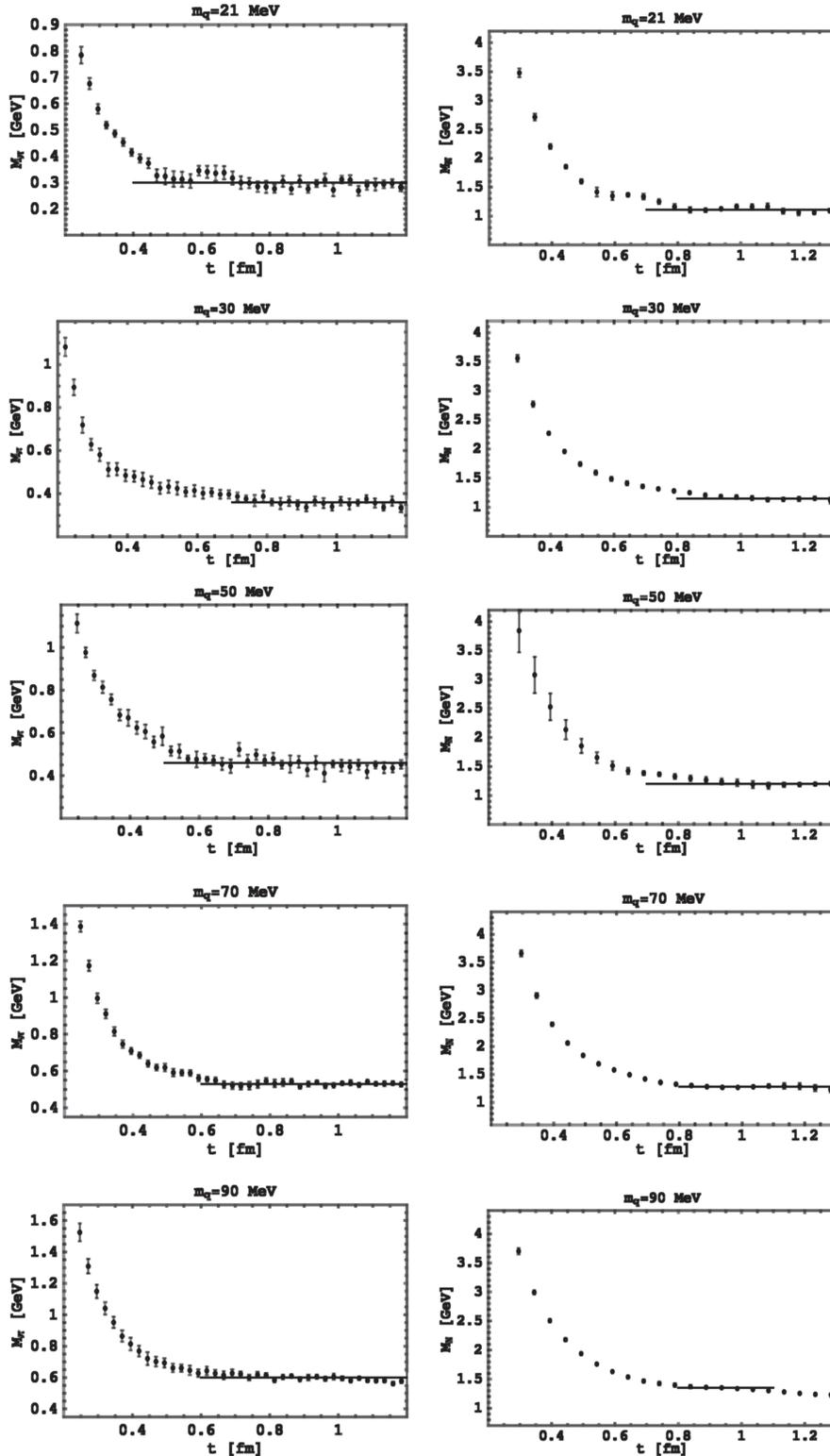
FIG. 3.   Pion and nucleon effective-mass plots in the IILM at different quark masses.
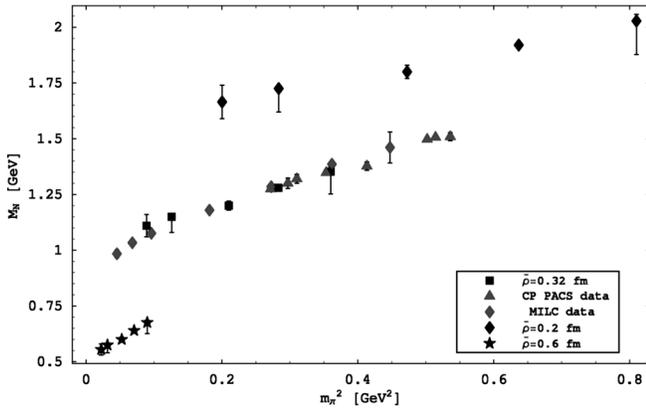
FIG. 4.   Comparison between nucleon masses obtained with the IILM for three different choices of the average instanton size $\bar{\rho}$ and those calculated on the Lattice by the CP-PACS [27] and MILC [28] collaborations.

V. CHIRAL EFFECTIVE PARAMETERS IN THE IILM

In the previous sections, we have shown that the IILM provides a realistic description of the microscopic dynamics responsible for chiral symmetry and that it contains

TABLE I.   Pion and nucleon masses fitted by effective-mass plot with $\chi^2/ndf \leq 1$. The quark masses are determined at a scale 2 GeV as in [33,34].

m_q [GeV]	Pion [GeV]	Nucleon [GeV]
0.021	0.300 ± 0.004	$1.11^{+0.05}_{-0.05}$
0.03	0.360 ± 0.004	$1.15^{+0.01}_{-0.07}$
0.05	0.460 ± 0.004	$1.20^{+0.02}_{-0.02}$
0.07	0.530 ± 0.004	$1.28^{+0.01}_{-0.01}$
0.09	0.600 ± 0.004	$1.35^{+0.02}_{-0.1}$
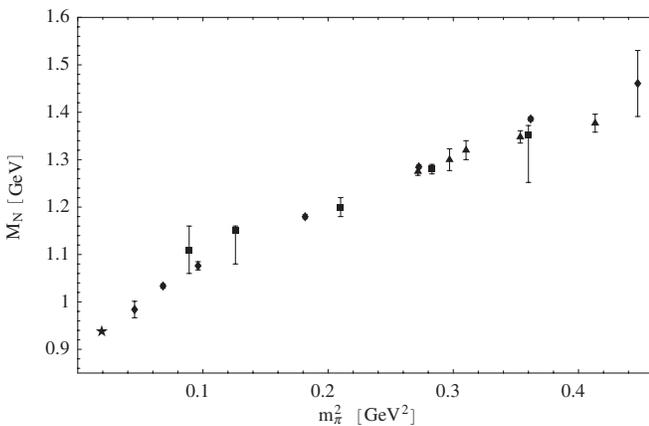
FIG. 5.   Nucleon mass: the IILM, CP-PACS, and MILC data are denoted by the squares, triangles, and diamonds, respectively, and the star represents the physical point.

pions as low-energy vacuum excitations. Thus, we conclude that the effective theory approximates the path integral sufficiently well that the IILM can be described by chiral perturbation theory, and we therefore ask the next question of how similar the low-energy constants are to those arising in QCD. Hence, we determine the quark condensate and the pion decay constant from the dependence of the pion mass on the quark mass. Note that the numerical value of the quark mass in QCD depends on the renormalization scale. In the IILM we do not have this freedom since the ultraviolet cut-off scale is provided by the inverse instanton size $1/\bar{\rho} \simeq 600$ MeV. Chiral perturbation theory to $\mathcal{O}(p^4)$ predicts a dependence of the form:

$$m_\pi^2 = 2m_q B_0 \left(1 + \frac{2m_q B_0}{32\pi^2 f_0^2} \ln\left(\frac{2mB_0}{\Lambda^2}\right)\right). \quad (36)$$

The chiral scale Λ is set at the ρ vector meson mass, which in this model is found to be independent on the quark mass, with the value $M_\rho = 1$ GeV [35]. Then, using the value for $\frac{B_0}{f_0^2} = 340$ GeV^{-1} which was extracted from the analysis of the Dirac spectrum (29), one can extract B_0.

The results of the chiral fit to the numerical IILM calculations are shown in Fig. 6. The corresponding low-energy chiral coefficients calculated in our model are

$$f_0 = 0.085 \pm 0.003 \text{ GeV}, \quad (37)$$

$$B_0 = 2.43 \pm 0.02 \text{ GeV}, \quad (38)$$

corresponding to a chiral condensate of

$$\langle \bar{q}q \rangle \approx -(0.259 \text{ GeV})^3. \quad (39)$$

The fact that these quantities are rather close to the corresponding values extracted in QCD implies that the low-energy effective theory of the IILM is indeed not far from that of QCD. Note that a recent analysis of the quark mass dependence of the chiral condensate in the instanton vacuum leading to comparable results can be found in [36].
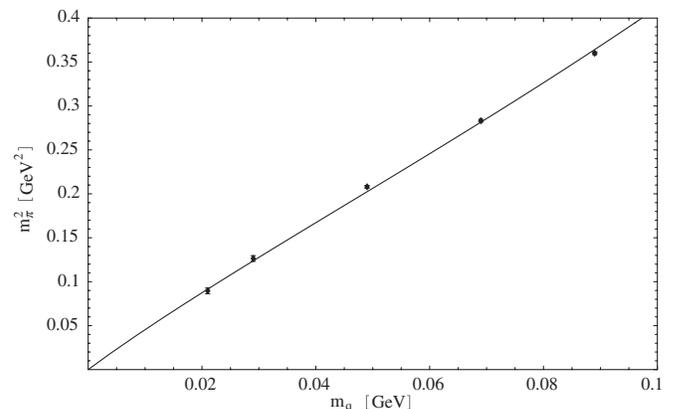
FIG. 6.   Chiral extrapolation of the pion mass, obtained in the IILM using $\mathcal{O}(p^4)$ χpt.

A similar analysis could in principle be carried out also in the nucleon sector, where several approaches to chiral extrapolation have been proposed, for example, see [37–41] and references therein. However, we prefer to avoid such an analysis, because the validity of the one-loop chiral extrapolation formulas for pion masses $\gtrsim 200$ MeV has been questioned [41] and is presently under debate.

VI. INSTANTON-INDUCED DYNAMICS IN THE CHIRAL REGIME

Having established that for $m_\pi \lesssim 500$ MeV the IILM agrees at a qualitative and even quantitative level with several QCD predictions obtained from χpt and lattice calculations, we can now use the physical insight from that model concerning the instanton-induced correlations to explore the dynamical mechanisms involved in the transition into the chiral regime.

From (16), it follows that the nonperturbative dynamics associated with the instanton-induced near-zero modes becomes parametrically small for quark masses much larger than the typical value of the overlap matrix element T_{IJ}. In Fig. 7 we have plotted the distributions of the *maximum* overlap matrix elements T_{IA} obtained at different values of the quark mass. We note that such distributions are peaked around the value $m^\star \simeq 80$ MeV. The value $m^\star$ plays a central role in specifying the scale for instanton-induced chiral symmetry breaking in the IILM. Physically, we expect that for $m_q \gg m^\star$, corresponding to $m_\pi \gg 500$ MeV, the interactions associated with chiral dynamics become subleading. We note that this number is consistent with the phenomenological estimate derived in [42], using the single-instanton approximation. To further illustrate this transition, in Fig. 8 we show the point-to-point pseudoscalar correlation function evaluated in the IILM in the zero-mode approximation (zma) in which

$$S(x, y) = S_{\text{free}}(x, y) + S_{zm}(x, y). \qquad (40)$$
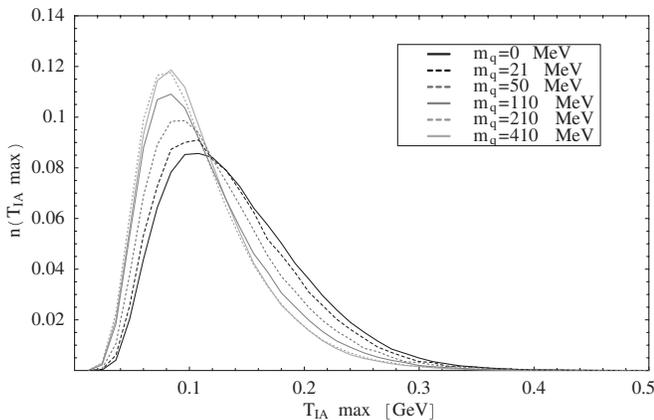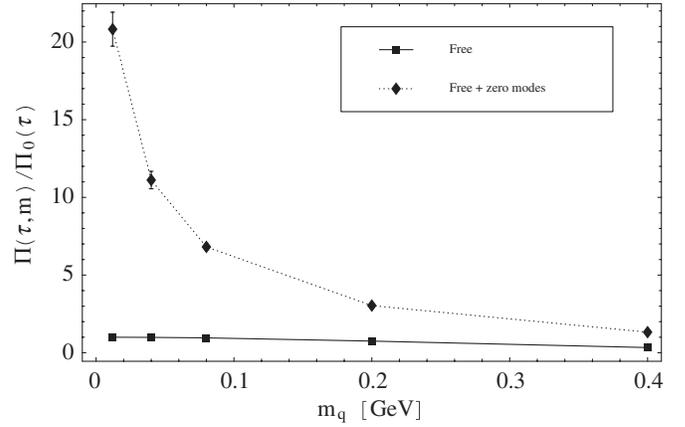
FIG. 8. Sum of the zero-mode and free contributions to the pseudoscalar point-to-point correlation function computed in the IILM at $\tau = 1$ fm for different quark masses (diamonds) compared with the free contribution alone (squares).

We normalize this full correlation function to the corresponding correlation computed in the free massless theory,

$$\frac{\Pi(\tau, m_q)}{\Pi_0(\tau)} = \frac{\langle 0|j_5(\tau)j_5^\dagger(0)|0\rangle_{\text{IILM-free}+zm}}{4\pi^4/\tau^6} \qquad (41)$$

$$j_5(x) = \bar{u}(x)\gamma_5 d(x), \qquad (42)$$

evaluated at a typical nonperturbative scale $\tau = 1$ fm for different quark masses, and compare it to the free massless theory without zero-mode contributions. We observe that for small quark masses, the contribution of the zero-mode part of the propagators completely saturates the propagator and is more than an order of magnitude larger than the free contribution. On the other hand, as the quark mass increases, the zero-mode contribution is gradually suppressed and for $m_q \simeq 200$ MeV it is only a few times larger than the free contribution.

As the quark mass gets larger and larger, the quark loop contribution to QCD correlation functions becomes more and more suppressed. Interestingly, in the IILM, the scale $m^\star$ also determines the regime where the quenched approximation is expected to become reliable. In fact, from Eqs. (12)–(14), we see that for quark masses $m_q \gg \max[T_{IJ}] \simeq m^\star$, the contribution of the overlap matrix elements to the fermionic determinant becomes negligible. On the other hand, in this model, the mass contribution to the ultraviolet sector of the spectrum factorizes and therefore cancels out in all ensemble averages.

The numerical results presented in the previous section reveal two interesting features of the Instanton Model: (i) for $m_q \lesssim m^\star$ the density of quasizero-modes increases as the quark mass decreases and (ii) for $m_q \gtrsim m^\star$ the near-zero-mode part of the spectrum becomes practically independent on the quark mass. These two nontrivial dynamical effects are in fact related and can be explained as follows. Quark loops are known to generate strong non-local correlations between pseudoparticles of opposite to-

FIG. 7. Distribution of the maximum fermionic overlap matrix elements in the IILM for different quark masses.

pological charge. Such correlations tend to suppress configurations in which one or more pseudoparticles are located far from all others. Hence, the contribution of the fermionic determinant leads to a reduction of the density of *nearly* zero-modes, as completely isolated instantons are known to have *exact* zero-modes. As the quark mass gets larger, such a topological screening becomes less and less effective and the population of near exact zero-modes increases, explaining the rise of the peak of eigenvalue density near the origin. On the other hand, we have seen in Sec. II that for $m_q \gtrsim m^*$, the contribution of the fermionic determinant is suppressed and fermion-induced topological screening completely disappears. As a result, the low-virtuality sector of the Dirac spectrum stops depending on the quark mass. These are interesting predictions of the instanton liquid model that can be checked with unquenched lattice calculations.

We conclude this section by emphasizing that the existence of a single mass scale m^* at which chiral symmetry breaking begins to diminish and at which the quenched approximating begins to become valid is a characteristic prediction of the instanton model. In principle, in full QCD we expect the scales for such transitions to be implicit functions of the only dimensional parameters of the theory, Λ_{QCD} and m_q and there is no *a priori* reason for which they should coincide, unless they are driven by a common dynamical mechanism.

VII. CONCLUSIONS

In this work we have used the IILM to investigate the dynamical mechanisms that drive the dynamics and the structure of hadrons in the light-quark sector of QCD. To this end, we have checked that the model's predictions are consistent with QCD in the pion mass regime $\lesssim 500$ MeV, where we expect chiral dynamics to play an important role. By computing the nucleon mass and pion mass at different values of the quark mass we have shown that the IILM is consistent with the existing lattice data in the range $m_\pi \sim$ 300–600 MeV. We have observed that the best agreement with lattice QCD data in this region is obtained for a value of the average instanton size $\bar\rho = 0.32$ fm, which is close to Shuryak's earlier phenomenological estimate. On the other hand, the calculated instanton density $n \approx 3$ fm^{-4} is considerably larger than in earlier phenomenological estimates and closer to lattice results. By studying the dependence on the quark mass of the density of eigenvalues of the Dirac operator, we have shown that the model also contains the correct dynamics to reproduce predictions of χpt in the small quark mass regime where such a theory is

applicable and finite-order calculations are reliable. We have shown that, in the chiral limit, our simulations converge to the $N_f = 2$ prediction: $\lim_{\lambda\to 0}\rho'(\lambda) = 0$. We have studied the modification of the Dirac spectrum induced by small quark masses and found that they are proportional to $m_q^\alpha \lambda^{1-\alpha}$, a functional form that generates a $1/m_q$ power-law divergence in the quark mass dependence of the scalar three-point correlators as predicted by χpt [22]. We have discussed how the qualitative structure of such mass corrections has a simple physical interpretation in terms of quark-loop-induced instanton-anti-instanton correlations. It would be very interesting to check if the corrections predicted in the IILM are observed in full lattice QCD simulations.

From a chiral extrapolation of the pion mass, we computed the effective chiral parameters f_π and B and showed that they are comparable to those in QCD.

Having checked that chiral dynamics is correctly incorporated in the instanton model, we have exploited our analytic understanding of instanton-induced correlations to study the dynamical mechanisms involved in the transition into the chiral regime at a microscopic level. We have identified a mass scale $m^* = 80$ MeV above which we do not expect QCD correlators to be dominated by chiral dynamics and above which quenched calculations should begin to approximate full QCD.

If the computational technology is developed to the point that the present statistical and systematic errors on the nucleon mass are significantly improved, this framework could represent a complementary tool to perform direct chiral extrapolation of a variety of observables of interest, such as moments of DIS and generalized parton distributions, magnetic moments and form factors. Another interesting development would be to investigate if unstable light-quark resonances that receive contribution at order n^2 level in the instanton density, such as the ρ-meson and Δ-isobar, can also be well described by the 't Hooft interaction. In this context it would also be interesting to investigate the effect of confinement on the hadron masses, extending the pseudoparticle ensemble to include both regular and singular-gauge instantons [43].

[1] T. Schaefer and E. Shuryak, Phys. Rev. D **53**, 6522 (1996).
[2] T. Schaefer and E. Shuryak, Rev. Mod. Phys. **70**, 323 (1998).
[3] D. Diakonov, Prog. Part. Nucl. Phys. **51**, 173 (2003).
[4] E. Shuryak, Nucl. Phys. **B203**, 93 (1982).
[5] J. W. Negele, Nucl. Phys. B, Proc. Suppl. **73**, 92 (1999).
[6] M. Chu, J. Grandy, S. Huang, and J. W. Negele, Phys. Rev. D **49**, 6039 (1994).
[7] T. A. DeGrand and A. Hasenfratz, Phys. Rev. D **64**, 034512 (2001).
[8] P. Faccioli and T. A. DeGrand, Phys. Rev. Lett. **91**, 182001 (2003).
[9] P. Boucaud *et al.*, J. High Energy Phys. 04 (2003) 005.
[10] C. Gattringer, M. Gockeler, P. Rakow, S. Schaefer, and A. Schafer, Nucl. Phys. **B617**, 101 (2001).
[11] C. Gattringer, Phys. Rev. Lett. **88**, 221601 (2002).
[12] P. Faccioli, Int. J. Mod. Phys. A **20**, 4615 (2005).
[13] E. Shuryak and J. Verbaarschot, Nucl. Phys. **B410**, 55 (1993).
[14] E. Shuryak and J. Verbaarschot, Nucl. Phys. **B412**, 143 (1994).
[15] P. Faccioli and E. Shuryak, Phys. Rev. D **65**, 076002 (2002).
[16] P. Faccioli, A. Schwenk, and E. Shuryak, Phys. Lett. B **549**, 93 (2002).
[17] P. Faccioli, Phys. Rev. C **69**, 065211 (2004).
[18] P. Faccioli, A. Schwenk, and E. Shuryak, Phys. Rev. D **67**, 113009 (2003).
[19] M. Cristoforetti, P. Faccioli, E. Shuryak, and M. Traini, Phys. Rev. D **70**, 054016 (2004).
[20] M. Cristoforetti, P. Faccioli, G. Ripka, and M. Traini, Phys. Rev. D **71**, 114010 (2005).
[21] D. Diakonov, hep-ph/9602375.
[22] A. Smilga and J. Stern, Phys. Lett. B **318**, 531 (1993).
[23] J. Verbaarschot, Nucl. Phys. **B362**, 33 (1991).
[24] E. V. Shuryak and J. J. M. Verbaarschot, Nucl. Phys. **B341**, 1 (1990).
[25] J. J. M. Verbaarschot, Nucl. Phys. **B427**, 534 (1994).
[26] T. Schaefer and E. Shuryak, Phys. Rev. D **54**, 1099 (1996).
[27] A. A. Khan *et al.*, Nucl. Phys. **B689**, 175 (2004).
[28] C. Aubin *et al.*, Phys. Rev. D **70**, 094505 (2004).
[29] D. A. Smith and M. Teper, Phys. Rev. D **58**, 014505 (1998).
[30] A. Hasenfratz and C. Nieter, Phys. Lett. B **439**, 366 (1998).
[31] P. de Forcand, M. G. Perez, J. E. Hetrick, and I. O. Stamatescu, hep-lat/9802017.
[32] T. L. Ivanenko and J. W. Negele, Nucl. Phys. B, Proc. Suppl. **63**, 504 (1998).
[33] M. Musakhanov, hep-ph/0104163.
[34] P. Bowman, U. M. Heller, D. B. A. Leinweber, and G. Williams, Nucl. Phys. B, Proc. Suppl. **119**, 323 (2003).
[35] M. Cristoforetti, P. Faccioli, J. Negele, and M. Traini (unpublished).
[36] H.-C. Kim, M. Musakhanov, and M. Siddikov, Phys. Lett. B **633**, 701 (2006).
[37] M. Procura, T. Hemmert, and W. Weise, Phys. Rev. D **69**, 034505 (2004).
[38] M. Procura, B. U. Munsch, T. Wollenweber, T. Hemmert, and W. Weise, Phys. Rev. D **73**, 114510 (2006).
[39] W. Detmold and M. J. Savage, Phys. Lett. B **599**, 32 (2004).
[40] D. B. Leinweber, A. W. Thomas, and R. D. Young, Nucl. Phys. A **755**, 59 (2005).
[41] V. Bernard, T. Hemmert, and U.-G. Meißner, Nucl. Phys. A **732**, 149 (2004).
[42] P. Faccioli and E. Shuryak, Phys. Rev. D **64**, 114020 (2001).
[43] F. Lenz, J. W. Negele, and M. Thies, Phys. Rev. D **69**, 074009 (2004).